An efficient kinetic modeling of electrons with nonlocal Ohm's law in plasmas relevant to inertial confinement fusion by using the AWBS transport equation

M. Holec,* V. Tikhonchuk, J.-L. Feugeas, and Ph. Nicolai

Centre Lasers Intenses et Applications,
Universite de Bordeaux-CNRS-CEA,
UMR 5107, F-33405 Talence, France.

P. Loiseau and A. Debayle

CEA, DAM, DIF, F-91297 Arpajon Cedex, France.

J. P. Brodrick, D. Del Sorbo, and C. P. Ridgers

York Plasma Institute, Department of Physics, University of York,
Heslington, York, YO10 5DD, UK.

B. Dubroca

, Universite de Bordeaux,
France.

R. J. Kingham

Plasma Physics Group, Blackett Laboratory, Imperial College,
London SW7 2BW, United Kingdom.

(Dated: November 7, 2018)

A preliminary version... The interaction of lasers with plasmas very often leads to nonlocal transport conditions, where the classical hydrodynamic model fails to describe physical phenomena, such as heat-flow, related to highly mobile particles. In this study the electron distribution in plasma is investigated for the conditions relevant to ICF. In particular, we focus on the transport of nonlocal (supra-thermal) electrons streaming down the temperature gradient in the ablating plasma. Nevertheless, the nature of plasma (ionized gas) requires a correct response of background electrons too. This is achieved by the action of an electric field, which provides a self-consistent Ohms law based on the kinetic modeling.Our approach leans on the Albritton-Williams-Bernstein-Swartz collision operator providing a simple, computationally efficient, transport equation of electrons and is further benchmarked against Vlasov-Fokker-Planck codes Aladin and Impact and collisional PIC code Calder.

I. INTRODUCTION

The first modern attempts at kinetic modeling of plasma can be traced back to the fifties, when Cohen, Spitzer, and Routly (CSR) [1] demonstrated that the effect of Coulomb collisions between electrons and ions in the ionized gas predominantly results from frequently occurring events of cumulative small deflections rather than occasional close encounters. This effect was originally described by Jeans in [2] and Chandrasekhar [3] proposed to use the diffusion equation model of the Vlasov-Fokker-Planck type (VFP) [4].

A classical paper by Spitzer and Harm (SH) [5] provides the computation of the electron distribution function (EDF) in a plasma (from low to high Z) with a temperature gradient accounting for e-e and e-i collisions. The resulting expressions for current and heat flux are widely used in plasma hydrodynamic models. The distribution function based on the spherical harmonics method in its first approximation (P1) [6] is of the form $f^0 + \mu f^1$,

where f^0 and f^1 are isotropic and μ, is the direction cosine between the particle trajectory and some preferred direction in space. It should be emphasized that the SH solution expresses a small perturbation of equilibrium, i.e. that f^0 is the Maxwell-Boltzmann distribution and μf^1 represents a very small anisotropic deviation. This approximation holds for $L_T \gg \lambda_e$, a condition which is often invalid in laser plasmas, where L_T is the temperature length scale and λ_e the mean free path of electrons. It is worth mentioning, that electrons having 3 to 4 times the thermal velocity are dominantly responsible for heat-flow and that those faster than 6 times the thermal velocity can be completely neglected in this local theory.

The actual cornerstone of the modern VFP simulations was set in place by Rosenbluth [7], when he derived a simplified form of the VFP equation for a finite expansion of the distribution function, where all the terms are computed according to plasma conditions, including f^0, which of course needs to tend to the Maxwell-Boltzmann distribution. Consequently, the pioneering work on numerical solution of the VFP equation [8, 9] revealed the importance of the nonlocal electron transport in laser-heated plasmas. In particular, that the heat

---

* holec1@llnl.gov

flow down steep temperature gradients in unmagnetised plasma cannot be described by the classical, local fluid description of transport [5, 10]. This is due to the classical f^1 is not a small deviation (especially for electrons having 3 to 4 times the thermal velocity), i.e. $f^0 \sim f^1$ characterized by $L_T \sim \lambda_e$. It was also shown that a thermal transport inhibition [8] around the peak of the temperature gradient, and a nonlocal preheat ahead of the main heat wave front, naturally appear. These effects are attributed to significant deviations of f^0 from Maxwellian distribution.

Nevertheless, numerical solution of the VFP equation even in the Rosenbluth formalism remains very challenging computationally, because the e-e collision integral is nonlinear. More simple linear forms of e-e collision operator are needed. Although some VFP simulations on experimentally relevant timescales have been performed (for recent examples see [11–17], an extensive review has been conducted by Thomas et al. [18]), their relative computational inefficiency severely limits the range of simulations that can be performed.

It is the purpose of this paper to present an efficient alternative to a full solution of the VFP equation to accurately calculate nonlocal transport, based on the Albritton-Williams-Bernstein-Swartz collision operator (AWBS) [19]. In Section II we propose a modified form of the AWBS collision operator, where its important properties are further presented in Section III with the emphasis on its comparison to the full VFP solution in local diffusive regime. Section V focuses on the performance of the AWBS transport equation model compared to modern kinetic codes including VFP codes Aladin and Impact [20], and PIC code Calder [21], where the cases related to real laser generated plasma conditions are studied. Finally, the most important outcomes of our research are concluded in Section VI.

II. THE AWBS KINETIC MODEL

The electrons in plasma can be modeled by the deterministic Vlasov model of charged particles

$$\frac{\partial f}{\partial t} + \boldsymbol{v} \cdot \nabla_{\boldsymbol{x}} f + \frac{q_e}{m_e} \left(\boldsymbol{E} + \frac{\boldsymbol{v}}{c} \times \boldsymbol{B} \right) \cdot \nabla_{\boldsymbol{v}} f = C_{ee}(f) + C_{ei}(f),$$
(1)

where $f(t, \boldsymbol{x}, \boldsymbol{v})$ represents the density function of electrons at time t, spatial point $\boldsymbol{x}$, and velocity $\boldsymbol{v}$, $\boldsymbol{E}$ and $\boldsymbol{B}$ are the electric and magnetic fields in plasma, q_e and m_e being the charge and mass of electron.

The general form of the e-e collision operator C_{ee} is the Fokker-Planck form published by Landau [22]

$$C_{FP}(f) = \Gamma \int \nabla_{\boldsymbol{v}} \nabla_{\boldsymbol{v}} (\boldsymbol{v} - \tilde{\boldsymbol{v}}) \cdot (f \nabla_{\tilde{\boldsymbol{v}}} f - f \nabla_{\boldsymbol{v}} f) \, \mathrm{d}\tilde{\boldsymbol{v}}, \quad (2)$$

where $\Gamma = \frac{4\pi q_e^4 \ln\Lambda}{m_e^2}$ and $\ln\Lambda$ is the Coulomb logarithm. The e-i collision operator C_{ei} could be expressed in a simpler form since massive ions are considered to be motionless compared to electrons during a collision. The scattering operator accounts for the change of electron velocity without change in the velocity magnitude , i.e. angular scattering. It is expressed in spherical coordinates as

$$C_{ei}(f) = \frac{\nu_{ei}}{2} \left(\frac{\partial}{\partial \mu} \left((1 - \mu^2) \frac{\partial f}{\partial \mu} \right) + \frac{1}{\sin^2 \phi} \frac{\partial^2 f}{\partial \theta^2} \right), \quad (3)$$

where $\mu = \cos\phi$, ϕ and θ are the polar and azimuthal angles, and $\nu_{ei} = \frac{Z n_e \Gamma}{v^3}$ is the e-i collision frequency.

The e-e collision operator needs to be linearized for efficient computation. Fisch introduced a linear form of C_{ee} in [23] in the high-velocity limit ($v \gg v_{th}$) electron collision operator

$$C_H(f) = v \nu_e \frac{\partial}{\partial v} \left(f + \frac{v_{th}^2}{v} \frac{\partial f}{\partial v} \right)$$
$$+ \frac{\nu_e}{2} \left(1 - \frac{v_{th}^2}{2v^2} \right) \left(\frac{\partial}{\partial \mu} \left((1 - \mu^2) \frac{\partial f}{\partial \mu} \right) + \frac{1}{\sin^2 \phi} \frac{\partial^2 f}{\partial \theta^2} \right),$$
(4)

where $\nu_e = \frac{n_e \Gamma}{v^3}$ is the e-e collision frequency and $v_{th} = \sqrt{\frac{k_B T_e}{m_e}}$ is the electron thermal velocity. The linear form of C_H arises from an assumption that the fast electrons predominantly interact with the thermal (slow) electrons, which is an important simplification to the form (2). However the diffusion term in the e-e collision operator (4) still presents numerical difficulties.

A yet simpler form of the collision operator of electrons was proposed in [24]

$$C_{AWBS}(f) = v \nu_e^* \frac{\partial}{\partial v} (f - f_M)$$
$$+ \frac{\nu_{ei} + \nu_e^*}{2} \left(\frac{\partial}{\partial \mu} \left((1 - \mu^2) \frac{\partial f}{\partial \mu} \right) + \frac{1}{\sin^2 \phi} \frac{\partial^2 f}{\partial \theta^2} \right), \quad (5)$$

where $f_M = \frac{n_e}{(2\pi)^{\frac{3}{2}} v_{th}^3} \exp\left(-\frac{v^2}{2 v_{th}^2} \right)$ is the Maxwell-Boltzmann equilibrium distribution. Here, the first term representing the AWBS operator [19] accounts for relaxation to equilibrium due to the e-e collisions, and the second term accounts for the e-i and e-e collisions contribution to scattering.

A method of angular momenta for the solution of the electron kinetic equation with the collision operator (5) was introduced in [24, 25].

In (5) we have introduced a modified e-e collision frequency ν_e^* in order to address a proper behavior with respect to Z, which is further analyzed in Section III and promising results compared to the full FP operator are presented.

III. BGK, AWBS, AND FOKKER-PLANCK MODELS IN LOCAL DIFFUSIVE REGIME

An approximate solution to the so-called *local diffusive regime* of electron transport can be found, since the *dif-*

fusive regime refers to a low anisotropy given by the projection μ. i.e. modeled by a simple P1 form of EDF

$$\tilde{f}(z,v,\mu) = f^0(z,v) + \mu f^1(z,v), \qquad (6)$$

where z is the spatial coordinate along the axis z, v the magnitude of transport velocity, and $\mu = \cos\phi$, where ϕ is the pitch angle with respect to the axis z.

The approximate transport solution is then obtained when analyzing the action of the time-steady form of (1) in 1D on the approximation (6) as

$$\mu\left(\frac{\partial\tilde{f}}{\partial z} + \frac{q_e E_z}{m_e v}\frac{\partial\tilde{f}}{\partial v}\right) + \frac{q_e E_z}{m_e}\frac{(1-\mu^2)}{v^2}\frac{\partial\tilde{f}}{\partial\mu} = \frac{1}{v}C(\tilde{f}), \quad (7)$$

where C is a given collision operator including both e-e and e-i collisions.

The locality of transport is the best expressed in terms of the Knudsen number $Kn = \frac{\lambda}{L}$, where λ is the mean free path of electron and L the characteristic length scale of plasma. Consequently, plasma conditions characterized by $Kn \ll 1$ exhibit a local transport regime. This measure then play a very important role in our analysis, where we use the electroni-electron and electron-ion mean free paths $\lambda_e = Z\lambda_{ei} = \frac{v}{\nu_e}$, and the density and temperature plasma scale lengths $L_{n_e} = n_e/\frac{\partial n_e}{\partial z}$ and $L_{T_e} = T_e/\frac{\partial T_e}{\partial z}$.

In practice, the Knudsen number of thermal electrons is often used as a measure of the locality of transport corresponding to given plasma conditions, where $Kn(v_{th}) < 0.001$ is considered the limit of validity of the local transport theory [26].

A. The BGK local diffusive electron transport

Bhatnagar, Gross, and Krook introduced a very simple form of a collision operator [27]

$$C_{BGK}(\tilde{f}) = \nu_e(\tilde{f} - f_M) + \frac{\nu_{ei} + \nu_e}{2}\frac{\partial}{\partial\mu}(1-\mu^2)\frac{\partial\tilde{f}}{\partial\mu}. \quad (8)$$

In spite of its simple form, BGK collision operator (8) serves as a useful model providing a relevant kinetic response, yet only qualitative with respect to the FP collision operator (2). In particular, the conservation of kinetic energy, momentum, and number of particles is often violated [28].

However, the form of (8) provides a simple analytical treatment of local diffusive transport regime, when used in (7). As a result, one finds a simple form of the BGK isotropic and anisotropic terms of (6) to be

$$f^0 = f_M + Kn\frac{v_{th}^2}{v^2}f^1, \qquad (9)$$

$$f^1 = -\frac{\lambda_e}{Z}\left(\frac{\partial f^0}{\partial z} + \frac{q_e E_z}{m_e v}\frac{\partial f^0}{\partial v}\right), \qquad (10)$$

where $Kn = \frac{\lambda_e}{L_{n_e}} + \frac{5}{2}\frac{\lambda_e}{L_{T_e}}$ and a detailed derivation of (9) and (10) can be found in Appendix A. Equation (9) states that $f^0 \to f_M$ when $Kn \ll 1$, and accordingly, $f^1 \to -\frac{\lambda_e}{Z}\left(\frac{\partial f_M}{\partial z} + \frac{q_e E_z}{m_e v}\frac{\partial f_M}{\partial v}\right)$. When the quasi-neutrality constraint imposed by $\boldsymbol{E}_L$ (A7) is used, one finally obtains the analytical BGK form of (6)

$$\tilde{f}_{BGK} = f_M - \mu\left(\frac{v^2}{2v_{th}^2} - 4\right)\frac{1}{Z}\frac{\lambda_e}{L_{T_e}}f_M, \qquad (11)$$

which recovers the Lorentz electron-ion collision gas model [29]. It should be noticed that f^0 equilibrates to f_M as $O(Kn^2)$ in (9), since $f^1 = \left(\frac{v^2}{2v_{th}^2} - 4\right)\frac{1}{Z}Kn f_M$.

The details about the BGK distribution function compared to other collision operators can be found in Section III D.

B. The AWBS local diffusive electron transport

Similarly to the BGK model, the AWBS collision operator 5 explicitly uses equilibration to the Maxwell-Boltzmann distribution f_M. On the other hand, AWBS originates from C_H, which is derived from the full FP operator (2). This makes the AWBS operator to be superior to the BGK operator, which is considered a purely phenomenological model.

If (5) is used in (7), one obtains the following equations governing the AWBS isotropic and anisotropic terms of (6)

$$\frac{\partial f^0}{\partial v} = \frac{\partial f_M}{\partial v} + Kn\frac{v_{th}^2}{v^2}\frac{f^1}{v}, \qquad (12)$$

$$\frac{\partial f^1}{\partial v} - \frac{Z+\zeta}{v\zeta}f^1 = \frac{\lambda_e}{v\zeta}\left(\frac{\partial f^0}{\partial z} + \frac{q_e E_z}{m_e v}\frac{\partial f^0}{\partial v}\right), \quad (13)$$

where ζ represents a scaling parameter defining the modified e-e collision frequency as $\nu_e^* = \zeta\nu_e$. A detailed derivation of (12) and (13) can be found in Appendix A. One observes that f^0 goes to Maxwellian when the local regime of transport is settled. Indeed, according to equation (12) the derivative $\frac{\partial f^0}{\partial v} \to \frac{\partial f_M}{\partial v}$ when $Kn \ll 1$ for any electron velocity, thus leading to $f^0 \to f_M$. Consequently, one finds the AWBS model equation for f^1 in local diffusive regime to be

$$\frac{\partial f^1}{\partial v} + \frac{Z+\zeta}{v\zeta}f^1 =$$
$$\frac{\lambda_e}{v\zeta}\left(\frac{1}{L_{n_e}} + \left(\frac{v^2}{2v_{th}^2} - \frac{3}{2}\right)\frac{1}{L_{T_e}} - \frac{q_e E_z}{m_e v_{th}^2}\right)f_M. \quad (14)$$

Since there is no simple analytical formula for f^1 solving (14), we adopt the implicit Euler numerical integration with $\Delta v < 0$, i.e. we integrate from high electron velocity ($v_{max} = 7v_{th}$) to the velocity equal to zero (using 10^4 steps). This mimics a particle deceleration due

to collisions. The correct numerical solution of (14) corresponds to an appropriate value of E_z leading to a zero current. As in the BGK case, the numerical solution of (14) reveals that $f^1 \sim Kn f_M$ and that f^0 equilibrates to f_M as $O(Kn^2)$ based on (12).

The details about the AWBS distribution function compared to other collision operators and a proper evaluation of the scaling parameter ζ can be found in Section III D.

C. The Fokker-Planck local diffusive electron transport

The solution to the 1D transport equation (7) using the Fokker-Planck collision operator (2) is very ambitious, as demonstrated in [1, 3, 7], fortunately, one can use the explicit evaluation of the electron distribution function published in [5], which takes the following form

$$f^1(z,v) = \frac{v_{2th}^4}{\Gamma Z n_e}$$
$$\left(2\tilde{D}_T \left(\frac{v}{v_{2th}} \right) + \frac{3}{2} \frac{\gamma_T}{\gamma_E} \tilde{D}_E \left(\frac{v}{v_{2th}} \right) \right) \frac{f_M}{T} \frac{\partial T_e}{\partial z}, \quad (15)$$

where $\tilde{D}_T(x) = ZD_T(x)/B$, $\tilde{D}_E(x) = ZD_E(x)/A$, γ_T, and γ_E are numerical values in TABLE I, TABLE II, and TABLE III in [5], and $v_{2th} = \sqrt{\frac{k_B T_e}{2m_e}}$.

One should be aware, that the solution of (7) equipped with the full FP collision operator reveals the importance of e-e Coulomb collisions, which is emphasized in the Z dependence of the distribution function, current, heat flux, electric field, etc. In particular, the latter exhibits the following dependence [5]

$$\boldsymbol{E} = \frac{m_e v_{th}^2}{q_e} \left(\frac{\nabla n_e}{n_e} + \left(1 + \frac{3}{2} \frac{Z + 0.477}{Z + 2.15} \right) \frac{\nabla T_e}{T_e} \right), \quad (16)$$

which for $Z \gg 1$ corresponds to the classical Lorentz electric field (A7).

D. Summary of the BGK, AWBS, and Fokker-Planck local diffusive transport

Ever since the SH paper [5], the effect of microscopic electron transport on the current $\int q_e \boldsymbol{v} \tilde{f} \, \mathrm{d}\boldsymbol{v}$ and the heat flux $\int \frac{m_e |\boldsymbol{v}|^2}{2} \boldsymbol{v} \tilde{f} \, \mathrm{d}\boldsymbol{v}$ in plasmas under local diffusive conditions has been understood. By overcoming some delicate aspects of the numerical solution to (2) presented in the CSR paper [1], the effect of electron-electron collisions was properly quantified and the correct dependence on Z of the heat flux $\boldsymbol{q}$ was approximated as [5, 30]

$$\boldsymbol{q} = \xi(Z) \, \boldsymbol{q}_L = \frac{Z + 0.24}{Z + 4.2} \boldsymbol{q}_L, \quad (17)$$

	$Z = 1$	$Z = 2$	$Z = 4$	$Z = 16$	$Z = 116$
$\bar{\Delta}\boldsymbol{q}_{AWBS}$	0.057	0.004	0.037	0.021	0.004
$\phi(Z)$	-0.037	-0.003	0.04	0.058	0.065

TABLE I. Relative error $\bar{\Delta}\boldsymbol{q}_{AWBS} = |\boldsymbol{q}_{AWBS} - \boldsymbol{q}_{SH}|/\boldsymbol{q}_{SH}$ of the $\nu_e^* = \frac{\nu_e}{2}$ scaling used in the AWBS model (5) showing the discrepancy (maximum 6%) with respect to the original solution of the heat flux given by numerical solution in Spitzer and Harm [5]. The values of $\phi(Z)$ (a weak dependence (19)) are also shown.

where $\boldsymbol{q}_L = \kappa T_e^{\frac{5}{2}} \nabla T_e$ is the heat flux given by the Lorentz gas model [29] and ξ the Z-dependence approximation. In the case of the BGK operator and its EDF formula (11), the correct dependence on Z can be simply achieved by scaling the e-e and e-i collision frequencies as

$$\nu_e^{BGK} = \frac{r\nu_e}{\xi}, \quad \nu_{ei}^{BGK} = \frac{\nu_{ei}}{\xi}, \quad (18)$$

which imposes a correct value of heat flux (17). The constant r in (18) has no effect on the local EDF as shown in Appendix A and can be set accordingly, e.g. to address the nonlocal transport behavior.

We have performed an extensive computational analysis in the case of the AWBS operator in order to obtain the heat flux behavior while varying Z. As expected, the heat flux magnitude did not match exactly the Z-dependence (17), e.g. for $Z = 1$ the AWBS heat flux was about 60% less than the SH calculation, while there was a perfect match in the case of $Z \gg 1$. By assuming that the e-e collisions are responsible for this inadequacy, we searched for a scaling of ν_e in (5). Interestingly, we found an almost constant scaling ζ, i.e. with a very weak dependency on Z as

$$\nu_e^* = \zeta(Z) \, \nu_e = \left(\frac{1}{2} + \phi(Z) \right) \nu_e \approx \frac{\nu_e}{2}, \quad (19)$$

where the dependence $\phi(Z) = \frac{0.59Z - 1.11}{8.37Z + 5.15} \ll \frac{1}{2}$ for any Z. Indeed, TABLE I shows $\phi(Z)$ and its corresponding relative error (maximum 6%) of the heat flux modeled by (5) vs. SH results represented by (17). It should be noted that the error is calculated with respect to original values presented in TABLE III in [5]. It is worth mentioning, that the zero current condition was followed in all AWBS calculations. The overall result is that the consistent electric field is always almost equal to the classical Lorentz value (A7) with the difference being less than 0.01 % for any Z.

Nevertheless, the electron-electron collisions effect represented by (17) provides only an integrated information

about the heat flux magnitude. If one takes a closer look at the distribution function itself, the conformity of the modified AWBS collision operator is even more emphasized as can be seen in FIG. 1 showing the flux moment in spherical coordinates of velocity

$$q_1 = \frac{m_e v^2}{2} v f^1 v^2. \tag{20}$$

In the case of the high Z Livermorium plasma ($Z = 116$), AWBS exactly aligns with the Lorentz gas limit. In the opposite case of the low Z Hydrogen plasma ($Z = 1$), the AWBS distribution function approaches significantly the numerical SH solution. BGK takes the Lorentz gas distribution function form for any Z only taking into account the scaling (18).
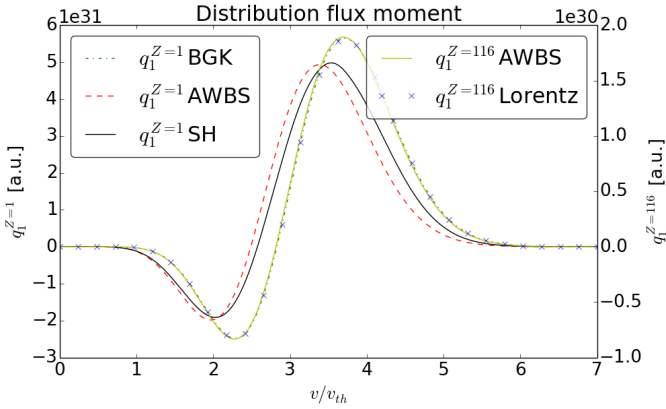

FIG. 1. The flux velocity moment of the anisotropic part of the electron distribution function in low $Z = 1$ and high $Z = 116$ plasmas in diffusive regime. In the case of $Z = 1$ the AWBS model matches very well the reference solution given by the SH calculation [5] in comparison to the BGK model. In the case of $Z = 116$ the AWBS model aligns exactly with the Lorentz gas approximation as expected. The BGK and the SH results are not shown, but correspond excatly to the Lorentz gas.

It is worth mentioning that the first derivative term in the AWBS collision operator (5) (red dashed line) provides a significant model improvement with respect to the SH (Fokker-Planck) solution (solid black line) compared to the simplest BGK model (8) (dashed-dot blue line) in FIG. 1.

IV. THE AWBS NONLOCAL TRANSPORT MODEL OF ELECTRONS

In order to define a nonlocal transport model of electrons, we use the AWBS collision operator and the P1 angular discretization of the electron distribution function

$$\tilde{f}(\boldsymbol{x}, \boldsymbol{n}, v) = f_0(\boldsymbol{x}, v) + \boldsymbol{n} \cdot \boldsymbol{f_1}(\boldsymbol{x}, v), \tag{21}$$

consisting of the isotropic part represented by the zeroth angular moment $f_0 = \frac{1}{4\pi} \int_{4\pi} \tilde{f} d\boldsymbol{n}$ and the directional part represented by the first angular moment $\boldsymbol{f_1} = \frac{3}{4\pi} \int_{4\pi} \boldsymbol{n} \tilde{f} d\boldsymbol{n}$, where $\boldsymbol{n}$ is the transport direction (the solid angle). Then, the first two angular moments [28] applied to the steady form of (1) with collision operator (5) (extended by (19)) lead to the model equations

$$v \frac{\nu_e}{2} \frac{\partial}{\partial v} (f_0 - f_M) = \frac{v}{3} \nabla \cdot \boldsymbol{f_1} + \frac{q_e}{m_e} \frac{\boldsymbol{E}}{3} \cdot \left(\frac{\partial \boldsymbol{f_1}}{\partial v} + \frac{2}{v} \boldsymbol{f_1} \right), \tag{22}$$

$$v \frac{\nu_e}{2} \frac{\partial \boldsymbol{f_1}}{\partial v} - \nu_{scat} \boldsymbol{f_1} = v \nabla f_0 + \frac{q_e}{m_e} \boldsymbol{E} \frac{\partial f_0}{\partial v} + \frac{q_e \boldsymbol{B}}{m_e c} \times \boldsymbol{f_1}, \tag{23}$$

where $\nu_{scat} = \nu_{ei} + \frac{\nu_e}{2}$. The system of equations (22) and (23) is called the **AP1 model** (AWBS + P1).

The AP1 model gives us information about the electron distribution function and a macroscopic interpretation of the microscopic EDF properties is of great importance providing the bridge between kinetic and fluid description of plasma. For example the *flux* quantities as electric current and heat flux due to the motion of electrons

$$\boldsymbol{j} = \frac{4\pi}{3} q_e \int v \boldsymbol{f_1} \, d\tilde{v}, \quad \boldsymbol{q_h} = \frac{4\pi}{3} \frac{m_e}{2} \int v^3 \boldsymbol{f_1} \, d\tilde{v},$$

where $d\tilde{v} = v^2 dv$ the spherical coordinates metric, are based on corresponding velocity moments (integrals) of the first angular moment of EDF. Consequently, the explicit formula for the first angular moment from (23) (the inversion inspired by [31]) proves to be extremely useful

$$\boldsymbol{f_1} = \frac{\nu_{scat}^2 \boldsymbol{F}^* + \boldsymbol{\omega}_B \, \boldsymbol{\omega}_B \cdot \boldsymbol{F}^* - \nu_{scat} \, \boldsymbol{\omega}_B \times \boldsymbol{F}^*}{\nu_{scat}(\boldsymbol{\omega}_B^2 + \nu_{scat}^2)}, \tag{24}$$

because it provides a valuable information about the dependence of macroscopic *flux* quantities on electric and magnetic fields in plasma, where $\boldsymbol{\omega}_B = \frac{q_e \boldsymbol{B}}{m_e c}$ is the electron gyro-frequency and $\boldsymbol{F}^* = v \frac{\nu_e}{2} \frac{\partial \boldsymbol{f_1}}{\partial v} - v \nabla f_0 - \frac{q_e}{m_e} \boldsymbol{E} \frac{\partial f_0}{\partial v}$.

A. Nonlocal Ohm's Law

The expression (24) becomes extremely useful when used to describe the electron fluid momentum, i.e. the current velocity moment

$$\boldsymbol{j}_{(f,\boldsymbol{E},\boldsymbol{B})} = q_e \int v \boldsymbol{f_1} v^2 \, dv =$$

$$- \frac{q_e^2}{m_e} \int v \frac{\nu_{ei}^2 \boldsymbol{E}^* + \boldsymbol{\omega}_B \, \boldsymbol{\omega}_B \cdot \boldsymbol{E}^* - \nu_{ei} \, \boldsymbol{\omega}_B \times \boldsymbol{E}^*}{\nu_{ei}(\boldsymbol{\omega}_B^2 + \nu_{ei}^2)} \, d\tilde{v},$$

where $\boldsymbol{E}^* = \boldsymbol{E} \frac{\partial f_0}{\partial v} + \frac{m_e}{q_e} v \nabla f_0$ is the effective electric field in plasma. This can be written as

$$\boldsymbol{j}_{(f,\boldsymbol{E},\boldsymbol{B})} = \mathbf{J}_{Ohm} \frac{\partial f_0}{\partial v} \boldsymbol{E} + \frac{m_e}{q_e} \mathbf{J}_{Ohm} v \nabla f_0, \tag{25}$$

where we used the following notation $\mathbf{J}_{Ohm}\boldsymbol{g} = -\frac{q_e^2}{m_e}\int v\frac{\nu_{ei}^2\boldsymbol{g}+\boldsymbol{\omega}_B\ \boldsymbol{\omega}_B\cdot\boldsymbol{g}-\nu_{ei}\ \boldsymbol{\omega}_B\times\boldsymbol{g}}{\nu_{ei}(\boldsymbol{\omega}_B^2+\nu_{ei}^2)}\ \mathrm{d}\tilde{v}$ showing how $\mathbf{J}_{Ohm}$ acts on a general vector field $\boldsymbol{g}$. We refer to (25) as to the **nonlocal Ohm's law**. The need for a nonlocal Ohm's law to accurately capture magnetic field advection by the Nernst effect has previously been demonstrated [12, 32, 33], although a full investigation of how well our new Ohm's law captures this is beyond the scope of this article.The proper local asymptotic to the standard Ohm's law can be found when $f_0 \to f_M$ and weak magnetization ($\boldsymbol{\omega}_B \ll \nu_{ei}$) is considered. Then (25) simplifies to

$$\boldsymbol{j} = -\frac{q_e^2}{m_e}\int\frac{v^3}{\nu_{ei}}\left(\boldsymbol{E}\ \frac{\partial f_M}{\partial v}+\frac{m_e}{q_e}v\nabla f_M\right)\ \mathrm{d}v =$$
$$\frac{16\sqrt{\frac{2}{\pi}}q_e^2 k_B^{\frac{3}{2}}T_e^{\frac{3}{2}}}{m_e^{\frac{5}{2}}\Gamma Z}\left[\boldsymbol{E}-\frac{\frac{5}{2}n_e k_B\nabla T_e+\nabla n_e k_B T_e}{q_e n_e}\right],\quad(26)$$

which can be directly compared to the local fluid theory

$$\boldsymbol{E}=\sigma(f_0)^{-1}\boldsymbol{j}-\frac{\nabla P(f_0)}{q_e n_e}\xrightarrow{f_0\to f_M}\boldsymbol{E}_l=\frac{\boldsymbol{j}}{\sigma_l}+\frac{\nabla p_e-\boldsymbol{R}_{T_e}}{q_e n_e},\quad(27)$$

while addressing properly the local electric field $\boldsymbol{E}_l$ given by the pressure $p_e = n_e k_B T_e$, the thermal force $\boldsymbol{R}_{T_e} = -\frac{3}{2}n_e k_B\nabla T_e$ and the local electrical conductivity $\sigma_l = 16\sqrt{\frac{2}{\pi}}q_e^2 k_B^{\frac{3}{2}}T_e^{\frac{3}{2}}/m_e^{\frac{5}{2}}\Gamma Z$ [10]. In (27) we defined the nonlocal electrical tensor conductivity

$$\sigma = \mathbf{J}_{Ohm}\frac{\partial f_0}{\partial v},\quad(28)$$

and the nonlocal microscopic force

$$\nabla P = \sigma^{-1}m_e n_e\mathbf{J}_{Ohm}v\nabla f_0,\quad(29)$$

based on (25).

The local dependence of the AP1 current (26) on electric field and gradients of n_e and T_e clearly demonstrates, that (27) is a local version of (25). This also implies that (25) provides a very important physics related to the magnetic field source in terms of nonlocal Biermann battery (similar to [34]), since the curl on the electric field (27) gives

$$\nabla\times\frac{\nabla P}{q_e n_e}\xrightarrow{f_0\to f_M}\nabla\times\frac{\nabla p_e-\boldsymbol{R}_{T_e}}{q_e n_e}=\frac{k_B}{q_e n_e}\nabla T_e\times\nabla n_e.\quad(30)$$

A local version of the **nonlocal Ohm's law** (25) compared to the *generalized Ohm's law* (27) when a magnetic field is applied would require a much more delicate analysis and we leave it as a future complementary work.

It should be noted, that ν_e-related terms in (24) have been omitted in (25), since the e-e collisions do not contribute (cancel out when integrated over velocity) to the momentum change, i.e. $\int v\left(v\frac{\nu_e}{2}\frac{\partial\boldsymbol{f_1}}{\partial v}-\frac{\nu_e}{2}\boldsymbol{f_1}\right)\mathrm{d}\tilde{v}=0$.

B. AWBS Nonlocal Magneto-Hydrodynamics

The *AWBS nonlocal magneto-hydrodynamic model* (Nonlocal-MHD) refers to two temperature single-fluid hydrodynamic model extended by a kinetic model of electrons using the AWBS transport equation, which provides a direct coupling between hydrodynamics and Maxwell equations.

Mass, momentum density, and total energy ρ, $\rho\boldsymbol{u}$, and $E = \frac{1}{2}\rho\boldsymbol{u}\cdot\boldsymbol{u}+\rho\varepsilon_i+\rho\varepsilon_e$, where ρ is the density of plasma, $\boldsymbol{u}$ the plasma fluid velocity, ε_i the specific internal ion energy density, and ε_e the specific internal electron energy density, are modeled by the Euler equations in Lagrangian frame [35, 36]

$$\frac{\mathrm{d}\rho}{\mathrm{d}t}=-\rho\nabla\cdot\boldsymbol{u},\quad(31)$$
$$\rho\frac{\mathrm{d}\boldsymbol{u}}{\mathrm{d}t}=-\nabla(p_i+p_e)+\boldsymbol{j}_{(f,\boldsymbol{E},\boldsymbol{B})}\times\boldsymbol{B},\quad(32)$$
$$\rho\,C_{V_i}\frac{\mathrm{d}T_i}{\mathrm{d}t}=\left(\rho^2 C_{T_i}-p_i\right)\nabla\cdot\boldsymbol{u}-G(T_i-T_e),\quad(33)$$
$$\rho\,C_{V_e}\frac{\mathrm{d}T_e}{\mathrm{d}t}=\left(\rho^2 C_{T_e}-p_e\right)\nabla\cdot\boldsymbol{u}+G(T_i-T_e)$$
$$-\nabla\cdot\boldsymbol{q}_{h(f,\boldsymbol{E},\boldsymbol{B})}+Q_{\mathrm{IB}},\quad(34)$$

where T_i is the temperature of ions, T_e the temperature of electrons, p_i the ion pressure, p_e the electron pressure, $\boldsymbol{q}_h$ the heat flux, Q_{IB} the inverse-bremsstrahlung laser absorption (which can also distort the distribution function away from a Maxwellian [37], strongly modifying the transport [38], an effect which will not be considered further here) and $G = \rho C_{V_e}\nu_{ei}$ is the ion-electron energy exchange rate. The thermodynamic closure terms p_e, p_i, $C_{V_i}=\frac{\partial\varepsilon_i}{\partial T_i}$, $C_{T_i}=\frac{\partial\varepsilon_i}{\partial\rho}$, $C_{V_e}=\frac{\partial\varepsilon_e}{\partial T_e}$, $C_{T_e}=\frac{\partial\varepsilon_e}{\partial\rho}$ are obtained from an equation of state (EOS), e.g. the SESAME equation of state tables [39, 40].

The magnetic and electric fields are modeled by Maxwell equations

$$\frac{1}{c}\frac{\mathrm{d}\boldsymbol{B}}{\mathrm{d}t}=-\nabla\times\boldsymbol{E},\quad(35)$$
$$\frac{1}{c}\frac{\mathrm{d}\boldsymbol{E}}{\mathrm{d}t}=\nabla\times\boldsymbol{B}-\frac{4\pi}{c}\boldsymbol{j}_{(f,\boldsymbol{E},\boldsymbol{B})},\quad(36)$$

where the initial state of $\boldsymbol{B}$ and $\boldsymbol{E}$ obeys the Gauss's law.

We have explicitly written the current and heat flux as dependent on electron kinetics, represented by the electron distribution function f, and electric and magnetic fields. In principal, $\boldsymbol{j}_{(f,\boldsymbol{E},\boldsymbol{B})}$ and $\boldsymbol{q}_{h(f,\boldsymbol{E},\boldsymbol{B})}$ can be referred to as the *kinetic closure* and is provided by the **AP1 model** (22) and (23), where f_M is given on the spatial profile of T_e governed by (34). All quantities are defined in the fluid frame in the aforementioned Nonlocal-MHD model.

C. Numerical Implementation of the AWBS Electron Kinetics

It is well known, that as the electron transport exhibits a quasi-steady behavior, the same holds for the electric field in (36) on the time scale of the fluid. Consequently, Ampere's law (36) usually takes a quasi-steady form $\frac{4\pi}{c}\boldsymbol{j}_{(f,\boldsymbol{E},\boldsymbol{B})} = \nabla \times \boldsymbol{B}$ when used in hydrodynamics. Proceeding further, one can make use of the **nonlocal Ohm's law** (25) to write a *fully kinetic form of Ampere's law* governing the electric field $\boldsymbol{E}$

$$\mathbf{J}_{Ohm}\frac{\partial f_0}{\partial v}\boldsymbol{E} + \frac{m_e}{q_e}\mathbf{J}_{Ohm}v\nabla f_0 = \frac{c}{4\pi}\nabla \times \boldsymbol{B}. \quad (37)$$

In order to solve the kinetics of electrons, we adopt a high-order finite element discretization [41, 42] of the model equations (22), (23), (37)

$$\mathbf{M}^{L_2}_{(\frac{v\nu_e}{2})} \cdot \frac{\mathrm{d}\boldsymbol{f_0}}{\mathrm{d}v} - \mathbf{V}^{L_2}_{(\frac{q_e\boldsymbol{E}}{3m_e})} \cdot \frac{\mathrm{d}\boldsymbol{f_1}}{\mathrm{d}v} = \mathbf{D}^{L_2}_{(\frac{v}{3})} \cdot \boldsymbol{f_1} + \mathbf{M}^{L_2}_{(\frac{2q_e\boldsymbol{E}}{3m_ev})} \cdot \boldsymbol{f_1}$$
$$+ \boldsymbol{b}^{L_2}_{(\frac{v\nu_e}{2}\frac{\partial f_M}{\partial v})}, \quad (38)$$

$$\mathbf{M}^{H_1}_{(\frac{v\nu_e}{2})} \cdot \frac{\mathrm{d}\boldsymbol{f_1}}{\mathrm{d}v} - \mathbf{V}^{H_1}_{(\frac{q_e\boldsymbol{E}}{m_e})} \cdot \frac{\mathrm{d}\boldsymbol{f_0}}{\mathrm{d}v} = \mathbf{G}^{H_1}_{(v)} \cdot \boldsymbol{f_0} + \mathbf{M}^{H_1}_{(\nu_{scat})} \cdot \boldsymbol{f_1}$$
$$+ \mathbf{C}^{H_1}_{(\frac{q_e\boldsymbol{B}}{m_ec}\times)} \cdot \boldsymbol{f_1}, \quad (39)$$

$$\mathbf{J}^{ND}_{(\frac{\partial f_0}{\partial v})} \cdot \boldsymbol{E} = \mathbf{JG}^{ND}_{(\frac{m_ev}{q_e})} \cdot \boldsymbol{f_0} + \boldsymbol{b}^{ND}_{(\frac{c}{4\pi}\nabla\times\boldsymbol{B})}, \quad (40)$$

where the continuous differential operators are represented by standard discrete analogs (matrices of bilinear forms) $\mathbf{M}, \mathbf{G}, \mathbf{D}, \mathbf{V}, \mathbf{C}$, i.e. mass, gradient, divergence, vector field dot product, and vector field curl, and by $\mathbf{J}, \mathbf{JG}$ matrices specific to **nonlocal Ohm's law** (25). The linear form $\boldsymbol{b}$ represents sources, i.e. temperature T_e via $\frac{\partial f_M}{\partial v}$ and the curl of the magnetic field $\boldsymbol{B}$. These finite element discrete analogs are defined on piece-wise continuous L_2 finite element space (domain of $\boldsymbol{f_0}$), continuous H_1 finite element space (domain of $\boldsymbol{f_1}$) [41], and Nedelec finite element space (domain of $\boldsymbol{E}$). We do not show their definitions since it is out of the scope of this article.

The strategy of solving (38) and (39) resides in integrating $\frac{\mathrm{d}\boldsymbol{f_0}}{\mathrm{d}v}$ and $\frac{\mathrm{d}\boldsymbol{f_1}}{\mathrm{d}v}$ along the velocity magnitude. This is done by starting the integration from infinite velocity ($v = 7v_{th}^{max}$ is a sufficiently high limit) to zero velocity using the Implicit Runge-Kutta method. The value v_{th}^{max} equals the electron thermal velocity corresponding to the maximum electron temperature in the current profile of plasma. It should be noted, that the backward integration concept is crucial for the model, since it corresponds to the deceleration of electrons due to collisions [43], which leads to some limitations described in Appendix B.

V. BENCHMARKING THE AWBS NONLOCAL TRANSPORT MODEL

After having shown several encouraging properties of the AWBS transport equation defined by (5) under local diffusive conditions in Sec. III, this section focuses on analyzing its behavior under nonlocal plasma conditions, extensively investigated in numerous publications [8, 24, 26, 44–47]. A variety of tests suitable for benchmarking the nonlocal electron transport models have been published [24, 25, 30, 48–50], we focus on conditions relevant to inertial confinement fusion plasmas generated by lasers.

We show results of our implementation of the AP1 nonlocal transport model presented in Sec. IV benchmarked against simulation results provided by a rather complete set of kinetic models with varying complexity. The most reliable model represents Calder, a collisional Particle-In-Cell code resolving the plasma frequency time scale, then a standard VFP model represented by Aladin and Impact [20], and last but not least we adopt the simplest kinetic approach represented by SNB nonlocal model [51] used on the hydrodynamic time scale. It should be stressed that it is a first time when a collisional PIC is used in benchmarking of nonlocal electron transport models.

Calder PIC code

A fluid description of the particle phase-space, including small angle binary collisions, can be described with the Maxwell equations (35), (36) coupled with the ion and electron Vlasov equations with the Landau-Beliaev-Budker collisions integral (LBB) [22, 52]

$$\frac{\partial f_\alpha}{\partial t} + \mathbf{v}\cdot\nabla_{\mathbf{x}}f_\alpha + q_\alpha\left(\mathbf{E} + \mathbf{v}\times\mathbf{B}\right)\nabla_{\mathbf{p}}f_\alpha =$$
$$C_{LBB}(f_\alpha, f_\alpha) + \sum_\beta C_{LBB}(f_\alpha, f_\beta). \quad (41)$$

The LBB collision integral takes the form

$$C_{LBB}(f_\alpha, f_\beta) =$$
$$-\frac{\partial}{\partial\mathbf{p}}\cdot\frac{\Gamma_{\alpha\beta}}{2}\left[\int \mathbf{U}(\mathbf{p}, \mathbf{p}')\cdot(f_\alpha\nabla_{\mathbf{p}'}f_\beta' - f_\beta'\nabla_{\mathbf{p}}f_\alpha)\right]d^3\mathbf{p}', \quad (42)$$

where its relativistic kernel reads $\mathbf{U}(\mathbf{p}, \mathbf{p}') = \frac{r^2/\gamma\gamma'}{(r^2-1)^{3/2}}$ $\left[(r^2-1)\mathbf{I} - \mathbf{p}\otimes\mathbf{p} - \mathbf{p}'\otimes\mathbf{p}' + r(\mathbf{p}\otimes\mathbf{p}' + \mathbf{p}'\otimes\mathbf{p})\right]$ with $\gamma = \sqrt{1+\mathbf{p}^2}$, $\gamma' = \sqrt{1+\mathbf{p}'^2}$ and $r = \gamma\gamma' - \mathbf{p}\cdot\mathbf{p}'$. The momemtum $\mathbf{p}_\alpha$ ($\mathbf{p}_\beta$) is normalized to $m_\alpha c$ (resp. $m_\beta c$). The collision operator (42) tends to (2) in the non-relativistic limit. The aforementioned model is solved in 3D by the PIC code CALDER. [21, 53].

Brief description of the Calder code FIG. 3.

Impact and Aladin VFP codes

The PIC code is extremely expensive as the collisions require the description of the velocity space in 3 dimensions. Yet, a reduction of dimensions can be done by

developing the distribution function in a cartesian tensor series, equivalent to a serie along the spherical harmonics [54]. This in its first order form corresponds to the P1 approximation (21) and coupled with the Landau-Fokker-Planck collisional operator (2) leads to the P_1-VFP model [20, 54]:

$$\frac{\partial f_0}{\partial t} + \frac{v}{3}\nabla \cdot \boldsymbol{f_1} + \frac{q_e}{3m_e v^2}\frac{\partial}{\partial v}(v^2\boldsymbol{E}\cdot\boldsymbol{f_1}) = C_{ee}^0(f_0), (43)$$

$$\frac{\partial \boldsymbol{f_1}}{\partial t} + v\nabla f_0 + \frac{q_e\boldsymbol{E}}{m_e}\frac{\partial f_0}{\partial v} + \frac{q_e\boldsymbol{B}}{m_e}\times\boldsymbol{f_1} = -\nu_{ei}\boldsymbol{f_1}. (44)$$

where for simplicity only a contribution of the isotropic part of the distribution function in (2) is used

$$C_{ee}^0(f_0) = \frac{\Gamma}{v^2}\frac{\partial}{\partial v}\left[C(f_0)f_0 + D(f_0)\frac{\partial f_0}{\partial v}\right], \quad (45)$$

$$C(f_0(v)) = 4\pi\int_0^v f_0(u)u^2\mathrm{d}u, \quad (46)$$

$$D(f_0 v)) = \frac{4\pi}{v}\int_0^v u^2\int_u^\infty w f_0(w)\mathrm{d}w\mathrm{d}u. \quad (47)$$

Impact and Aladin solve the system (43) and (44) with the Maxwell equations (35) and (36) in two dimensions, assuming motionless ions.

It is worth mentioning that AP1 uses similar model equations as Aladin and Impact with the difference, that AP1 describes the electron distribution function as quasi steady with respect to the time evolution of ion fluid, and of course, AP1 is using a simple (linear) collision operator inherently coupled to ion fluid via f_M.

Brief description of the Aladin code FIG. 4, FIG. 2.

SNB approach

Now considered as a standard among nonlocal electron models in hydrodynamic codes, SNB [51] represents an efficient P1 method based on the velocity dependent form of the collision BGK operator. It uses EDF approximation representing deviation from the local BGK theory

$$\tilde{f} = f_M + \delta f_0 + \boldsymbol{n}\cdot(\boldsymbol{f_{1M}} + \delta\boldsymbol{f_1}). \quad (48)$$

The zero and first angular moment of electron transport equation with scaled (18) collision operator (8) acts on SNB approximation (48) as (similar to (22) and (23))

$$\frac{r\nu_e}{\xi}\delta f_0 = -\frac{v}{3}\nabla\cdot\delta\boldsymbol{f_1} - \frac{v}{3}\nabla\cdot\boldsymbol{f_{1M}}$$
$$\underbrace{-\frac{q_e}{m_e}\frac{\boldsymbol{E}}{3}\cdot\left(\frac{\partial\boldsymbol{f_{1M}}}{\partial v} + \frac{\partial\delta\boldsymbol{f_1}}{\partial v} + \frac{2}{v}(\boldsymbol{f_{1M}} + \delta\boldsymbol{f_1})\right)}, \quad (49)$$

$$\frac{\nu_{ei}}{\xi}\delta\boldsymbol{f_1} = -v\nabla\delta f_0 - \frac{q_e}{m_e}\boldsymbol{E}\frac{\partial\delta f_0}{\partial v}$$
$$\underbrace{-\frac{\nu_{ei}}{\xi}\boldsymbol{f_{1M}} - v\nabla f_M - \frac{q_e}{m_e}\boldsymbol{E}\frac{\partial f_M}{\partial v}}_{= 0\ defines\ \boldsymbol{f_{1M}}},$$
$$\quad (50)$$

where the magnetic field was nglected. The underbraced part of (50) defines the local anisotropic term

$$\boldsymbol{f_{1M}} = -\frac{\xi v f_M}{\nu_{ei}}\left(\frac{\nabla n_e}{n_e} + \left(\frac{v^2}{2v_{th}^2} - \frac{3}{2}\right)\frac{\nabla T_e}{T_e} - \frac{q_e}{m_e v_{th}^2}\boldsymbol{E}\right). \quad (51)$$

The efficiency of SNB resides in omitting the directional electric field effect (crossed out terms in (49) and (50)), which leads to a simple diffusion model

$$\frac{1}{\lambda_e^{SNB}}\delta f_0 - \nabla\cdot\frac{\lambda_{ei}^{SNB}}{3}\nabla\delta f_0 = \nabla\cdot\frac{\xi\lambda_{ei}}{3}f_M\left(\frac{\nabla n_e}{n_e} + \frac{\nabla T_e}{T_e}\right), \quad (52)$$

where $\frac{1}{\lambda_{ei}^{SNB}} = \frac{\nu_{ei}}{\xi v} + \frac{|q_e\boldsymbol{E}|}{\frac{1}{2}m_e v^2}$ and $\lambda_e^{SNB} = \frac{\xi v}{r\nu_e}$, and the source term based on $\boldsymbol{f_{1M}}$ simplifies by avoiding the v-dependent bracket and the electric field effect in (51). The missing directional effect of $\boldsymbol{E}$ in (52) is mimicked as an isotropic scattering in defintion of λ_{ei}^{SNB} [51]. Consequently, the real directional effect of the electric field in SNB is reflected only via $\boldsymbol{f_{1M}}$. A self consistent zero current condition $\boldsymbol{j} = q_e\int v(\boldsymbol{f_{1M}} + \delta\boldsymbol{f_1})\,\mathrm{d}\tilde{v} = 0$ then defines the actual value of the electric field from (50) as

$$\boldsymbol{E} = -\frac{\int\frac{\xi v^2}{\nu_{ei}}\nabla(f_M + \delta f_0)\,\mathrm{d}\tilde{v}}{\int\frac{\xi v}{\nu_{ei}}\frac{q_e}{m_e}\frac{\partial f_M}{\partial v}\,\mathrm{d}\tilde{v}} = \boldsymbol{E_L} - \frac{\int\frac{v^2}{\nu_{ei}}\nabla\delta f_0\,\mathrm{d}\tilde{v}}{\frac{q_e}{m_e}\int\frac{v}{\nu_{ei}}\frac{\partial f_M}{\partial v}\,\mathrm{d}\tilde{v}}, \quad (53)$$

In this paper we porpose to use $r = \frac{1}{2}$ in accordance with (19). This choice gives $\lambda_e^{SNB} = \frac{v}{2.097\nu_e}$ in the case of $Z = 1$, which is in a very good accordance with $\lambda_e^{SNB} = \frac{v}{2\nu_e}$ proposed in [50]. The explicit form of the anistropic part of EDF then takes the form $\boldsymbol{f_1} = \boldsymbol{f_{1M}} - \lambda_{ei}^{SNB}\nabla\delta f_0$.

A. Heat-bath problem

The accuracy of the AP1 is compared to Calder, Aladin, Impact, and SNB by calculating the heat flow in the case where a large relative temperature variation

$$T_e(z) = 0.575 - 0.425\tanh\left((z - 450)s\right), \quad (54)$$

which exhibits a smooth steep gradient at point 450 μm connecting a hot bath ($T_e = 1$ keV) and cold bath ($T_e = 0.17$ keV) and s is the parameter of steepness. This test is referred to as a simple non-linear heat-bath problem and originally was introduced in [48] and further investigated in [24, 25, 49, 50].

The total computational box size is 700 μm in the case of Aladin and Impact and 1000 μm in the case of Calder. We performed Aladin, Impact, and Calder simulations showing an evolution of temperature starting from the initial profile (54). Due to the initial distribution function being approximated by a Maxwellian, the first phase of the simulation exhibits a transient behavior of the heat flux. After several ps the distribution adjusts properly to its nonlocal nature and the heat flux profiles can be usefully compared. We then take the temperature profile from Aladin/Impact/Calder and used our
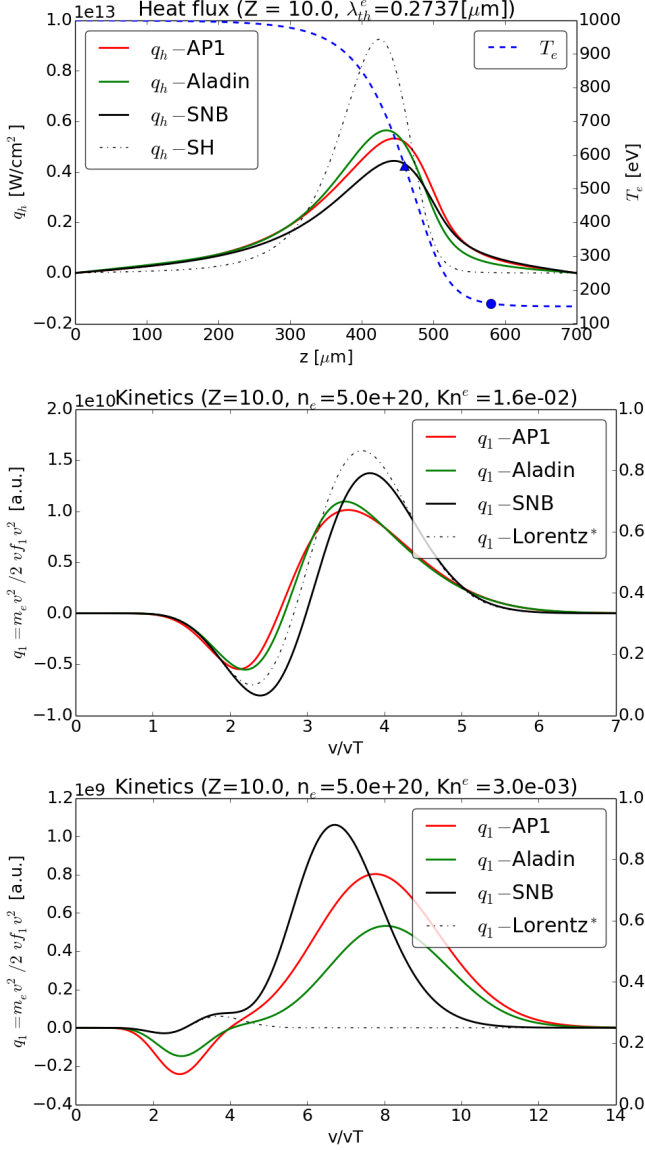
FIG. 2. Snapshot 12 ps. Top: correct steady solution of heat flux. Middle: correct comparison to kinetic profiles at point 460 μm by Aladin. Velocity limit 3.3 v_{th} at temperature 569.2 eV. Bottom: correct comparison to kinetic profiles at point 580 μm by Aladin. Velocity limit 13.1 v_{th} at temperature 159.4 eV.
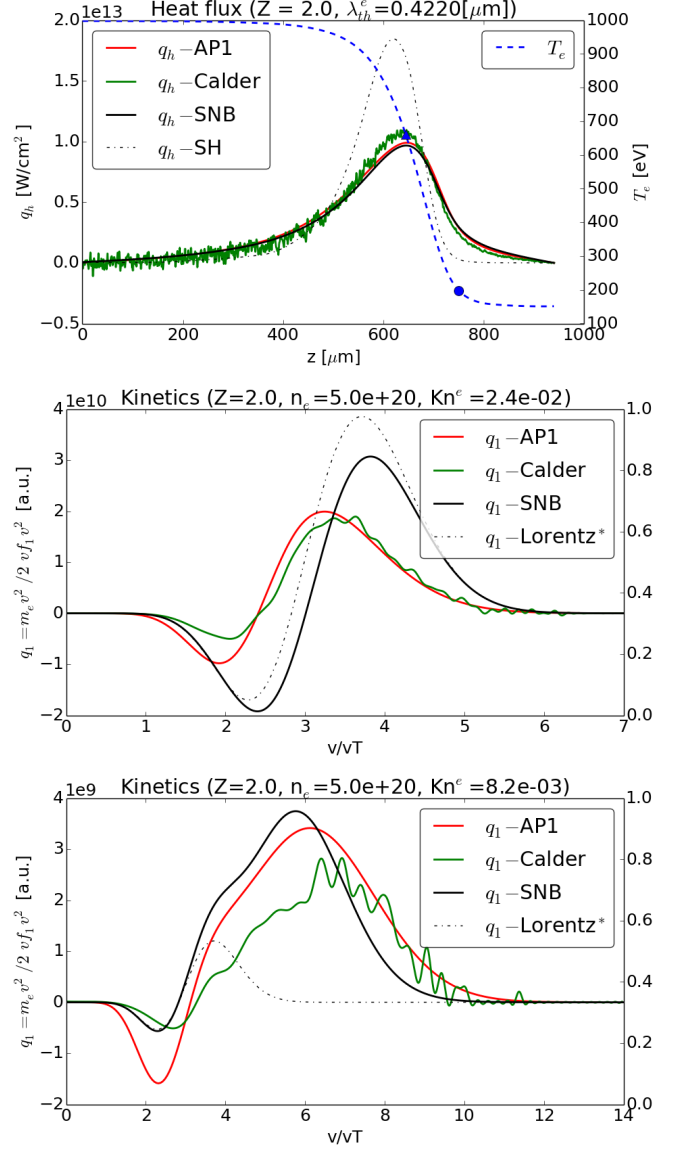
FIG. 3. Snapshot 11 ps. Top: correct steady solution of heat flux. Middle: correct comparison to kinetic profiles at point 640 μm by Calder. Velocity limit 3.8 v_{th} at temperature 662.3 eV. Bottom: correct comparison to kinetic profiles at point 750 μm by Calder. Velocity limit 7.4 v_{th} at temperature 198.0 eV.

AP1 and SNB implementations to calculate the heat flow they would predict given this profile. For all heat-bath simulations the electron density, Coulomb logarithm and ionisation were kept constant and uniform. The coulomb logarithm was held fixed throughout, $\ln\Lambda = 7.09$.

We show AP1 results for various ionization states, namely $Z = 10, 2, 1$ in FIG. 2, FIG. 3, and FIG. 4 respectively, corresponding to a moderate nonlocality ($\mathrm{Kn}^e \sim 10^{-2}$) leading to a rouhgly 50 % inhibition compared to the local SH heat flux maximum. It is preferable to use $\mathrm{Kn}^e = \frac{\lambda_e}{\sqrt{Z+1}L_{T_e}}$ instead of $\mathrm{Kn} = \frac{\lambda_{ei}}{L_{T_e}}$, because

$\sqrt{Z+1}$ provides a better scaling of nonlocality with respect to ionization [26], i.e. the flux inhibition and Kn^e are kept approximately the same when varying Z. In addition to the heat flux profiles, we also show the distribution function details related to the point of the heat flux maximum (644 μm) and to the point of the nonlocal transport effect (750 μm) in the form of the flux moment of EDFs anisotropic part (20). The nonlocal transport effect shows a very good agreement with previous results published in [49].

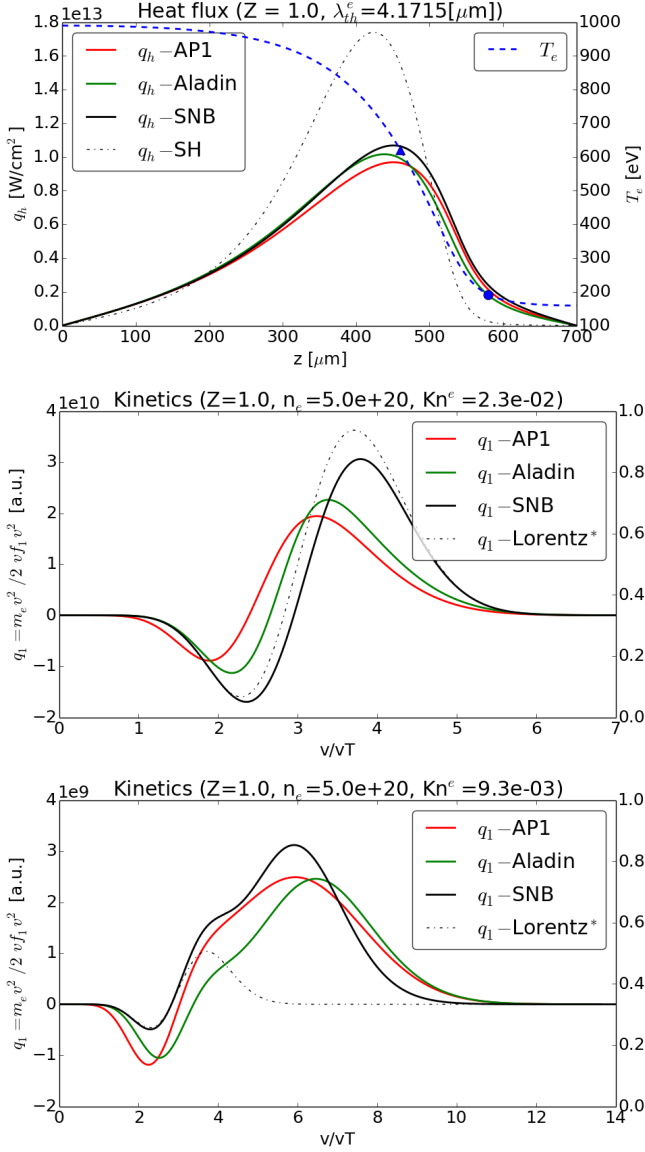In the top plot of FIG. 2 we show heat flux profiles

FIG. 4. Snapshot 20 ps. Top: correct steady solution of heat flux and electric field. Middle: correct comparison to kinetic profiles at point 460 μm by Aladin. Velocity limit 4.2 v_{th} at temperature 622.4 eV. Bottom: correct comparison to kinetic profiles at point 580 μm by Aladin. Velocity limit 9.1 v_{th} at temperature 192.3 eV.

computed by Aladin and AP1 corresponding to the temperature T_e profile computed by Aladin for $Z = 10$. The EDFs q_1 at the crossed point of the temperature profile is shown in the middle plot, where a very precise match between AP1 and Aladin can be observed, and q_1 at the circled point of the temperature profile is shown in the bottom plot. In the latter case AP1 shows a very similar properties as Aladin with a difference in magnitude corresponding to a higher heat flux computed by AP1 at this point.

In the top plot of FIG. 3 heat flux profiles computed by Calder and AP1 corresponding to the temperature T_e profile computed by Calder are shown for $Z = 2$. Very good match of q_1 can be seen between AP1 and Calder at the crossed point of the temperature profile in the middle plot and q_1 at the circled point of the temperature profile is shown in the bottom plot. In the latter case AP1 shows a very similar properties as Calder with a difference in magnitude corresponding to a higher heat flux computed by AP1 at this point. In general, Calder exhibits a lack of return current (negative part of q_1), i.e. the electron number is not exactly conserved. This probably arises from the nature of the Monte Carlo method used to solve (42) and its sensitivity to Gauss law of charge conservation.

Similar to FIG. 2, but for $Z = 1$, the heat flux profiles, q_1 at the heat flux maximum (crossed point) and at the nonlocal transport region (circled point) computed by Aladin and AP1 are shown in FIG. 4. It should be noted, that the difference in q_1 resembles to the low Z trend shown in FIG. 1 and that AP1 compares very well to Aladin. We also add the electric field profiles in the top plot of FIG. 4. One can see that $\boldsymbol{E}$ does not change much in magnitude, but it is displaced in direction down the temperature gradient thus causing a significant modification compared to the local $\boldsymbol{E}_L$ values. In general, a very good performance of AP1 model equations (22), (23), and (37) (no B field in 1D) can be observed in all three cases when compared to the computed results by Aladin and Calder.

In addition, the Knudsen number Kn^e has been varied among the simulation runs in order to address a broad range of nonlocality of the electron transport corresponding to the laser-heated plasma conditions, i.e. $Kn^e \in (0.0001, 1)$. The variation of Kn^e arises from the variation of the uniform electron density $n_e \in (10^{19}, 10^{23})$ cm^{-3} or the length scale given by the slope of the temperature profile $s \in (1/2500, 1/25)\mu$m. Results of an extensive set of simulations of varying Kn^e is shown in FIG. 5.

When analyzing the results of FIG. 5 we have found an important observation related to the stopping effect of electrons. It turns out, that the force acting on electrons is dominated by directional electric field above some velocity limit v_{lim} and this limit drops down significantly when the plasma conditions are more nonlocal, i.e. with increasing Knudsen number as can be seen in TABLE II. As a consequence, one can see that when $Kn^e \sim 10^{-1}$ the electrons responsible for the heat flux (velocity ~ 3.5 v_{th}) are preferably affected by the electric field rather than by collisions.

Yet another observation can be made when analysing q_1 in FIG. 2, FIG. 3, and FIG. 4. When comparing their middle and bottom plots, both velocity maxima of the EDF correspond to approximately same velocity for each of the cases, i.e. that the electrons responsible for the flux in the bottom plot are those flux dominating electrons from the heat flux maximum point shown in the middle plot. Notice that different reference temperatures and v_{th} are used in the middle and bottom plots.
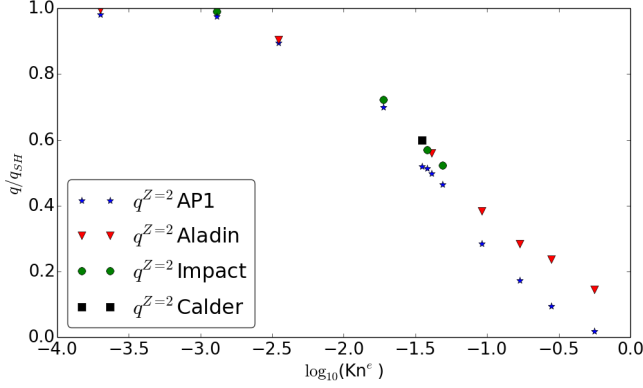
FIG. 5. Simulation results for the case $Z = 2$ computed by AP1/Aladin/Impact/Calder. Every point corresponds to the maximum heat flux in a "tanh" temperature simulation, which can be characterized by Kn. The range of $\log_{10}(Kn) \in (0, -4)$ can be expressed as equivalent to the electron density approximate range $n_e \in (1e19, 3.5e22)$ of the 50 μm slope tanh case. In the case of $Kn = 0.56$, $q_{Aladin}/q_{AP1} \approx 7.9$.

Kn^e	10^{-4}	10^{-3}	10^{-2}	10^{-1}	1
v_{lim}/v_{th}	70.8	22.4	7.3	3.1	1.8

TABLE II. Scan over varying nonlocality (Kn^e) showing the limit of the collision friction dominance over the acceleration of electrons due to the electric field force. The electric field effect is dominant for electrons with higher velocity than v_{lim} defined in (B3). Kn^e and v_{th} are evaluated from the same plasma profiles.

This provides a microscopic information about the motion of electrons on the nonlocal spatial scale.

In every simulation run of AP1 we used 250 velocity groups in order to avoid numerical errors in modeling of the electron kinetics. However, a smaller number of groups, e.g. 50, provides a very similar results (an error around 10% in the heat flux). *Here gather and provide a brief summary about the simulation input of Aladin, Impact, and Calder.*

B. Hohlraum problem

Additionally to the steep temperature gradients, the laser-heated plasma experiments also involve steep density gradients and variation in ionization, which is even more dominant in multi-material targets as in inertial fusion experiments, e.g. at the interface between the helium gas-fill and the ablated high Z plasma.

In [50], a kinetic simulation of such a test was intro-duced. Plasma profiles provided by a HYDRA simulation in 1D spherical geometry of a laser-heated gadolinium hohlraum containing a typical helium gas-fill were used as input for the IMPACT [20] VFP code. For simplicity, the Coulomb logarithm was treated as a constant $\ln\Lambda_{ei} = \ln\Lambda_{ee} = 2.1484$. In reality, in the low-density corona $\ln\Lambda$ reaches 8, which, however, does not affect the heat flux profile significantly. Plasma profiles at 20 nanoseconds of the HYDRA simulation were used (after spline smoothing) as the initial conditions for the IMPACT run (in planar geometry).

FIG. 6 shows the electron temperature T_e evolved during 10 ps by Impact, and the electron density n_e and ionization Z profiles. Along with plasma profiles the heat flux profiles of AP1, Impact, and SNB are also shown. *Kn profile will be probably added.* One can observe an overall good match among models in the preheat region.
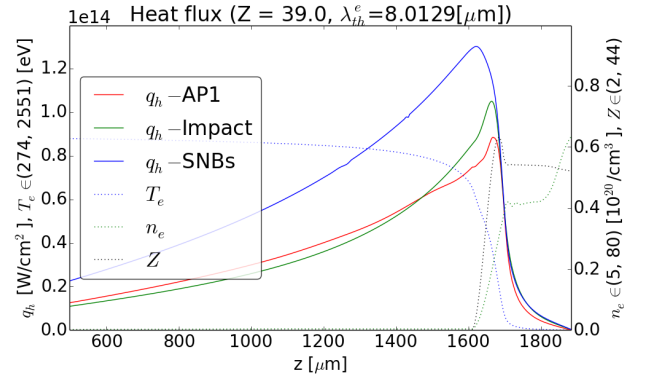

FIG. 6. Heat flux profiles by AP1, Impact and SNB along the electron temperature T_e, electron density n_e, and ionization Z profiles in a laser-heated gadolinium hohlraum containing a helium gas-fill.

It is worth mentioning that in the surroundings of the heat flux maximum ($\sim 1662\mu$m) the profiles of all plasma variables exhibit steep gradients with a change from $T_e = 2.5$ keV, $n_e = 5 \times 10^{20}$ cm^3, $Z = 2$ to $T_e = 0.3$ keV, $n_e = 6 \times 10^{21}$ cm^3, $Z = 44$ across approximately 100 μm (between 1600 μm and 1700 μm), starting at the helium-gadolinium interface. In this region, we can see a qualitative match between AP1 and Impact, however, we observe that the electric field limit Appendix B leads to the drop of the AP1 heat flux on the material interface, which then aligns to the Impact heat flux in the corona appropriately. On the other hand, SNB exhibits a significant heat flux overestimation in both the steep gradients region and in the plasma corona. We also attribute this to the lack of proper action of the electric field (the directional effect) in the SNB approach.

VI. CONCLUSIONS

- The most important point is that we introduce a collision operator, which is coherent with the full FP, i.e. no extra dependence on Z.

- Touch pros/contras of linearized FP in Aladin and Impact vs AWBS

- Raise discussion about what is the weakest point of AP1 for high Kns: the velocity limit or phenomenological Maxwellization?

- Summarize useful outcomes related to plasma physics as the competition between collisions and electric field in the electron stopping, then the knowledge about the nonlocal electron population (preheat electrons can be tracked back to the point of source according to their dominant velocity), and the last information about the tendency of the velocity maximum in q_1 with respect to Z and Kn^e.

- Emphasize the good results of Aladin (compared to Impact) and also outstanding results of Calder while being PIC.

- Electric field plays an important role in nonlocal electron kinetics and nonlocal Ohm's law provides the necessary equation to treat it properly.

- In coherence with the latter, the dfdv must be treated properly in nolocal electron kinetics, and so, AWBS can be included without any extra effort thus making it way much suitable than BGK, which is outperformed by AWBS when compared to FP.

ACKNOWLEDGMENTS

Appendix A: Background of the local diffusive regime theory

The left hand side of (7) acts on (6) as

$$\mu \left(\frac{\partial \tilde{f}}{\partial z} + \frac{q_e E_z}{m_e v} \frac{\partial \tilde{f}}{\partial v} \right) + \frac{q_e E_z}{m_e} \frac{1 - \mu^2}{v^2} \frac{\partial \tilde{f}}{\partial \mu} =$$
$$\mu \left(\frac{\partial f^0}{\partial z} + \frac{q_e E_z}{m_e v} \frac{\partial f^0}{\partial v} \right) + \frac{q_e E_z}{m_e v^2} f^1 + O(\mu^2). \quad (A1)$$

The action on (6) of the BGK operator (8) as used in (7) reads

$$\frac{1}{v} C_{BGK}(\tilde{f}) = \frac{\tilde{f} - f_M}{\lambda_e} + \frac{1}{2} \left(\frac{Z}{\lambda_e} + \frac{1}{\lambda_e} \right) \frac{\partial}{\partial \mu} (1 - \mu^2) \frac{\partial \tilde{f}}{\partial \mu},$$
$$= \frac{f^0 - f_M}{\lambda_e} - \mu \frac{Z}{\lambda_e} f^1. \quad (A2)$$

Consequently, if the isotropic and anisotropic parts of (A1) and (A2) are compared, one finds the following equations

$$f^0 = f_M + \frac{\lambda_e q_e E_z}{m_e v^2} f^1, \quad (A3)$$

$$f^1 = -\frac{\lambda_e}{Z} \left(\frac{\partial f^0}{\partial z} + \frac{q_e E_z}{m_e v} \frac{\partial f^0}{\partial v} \right). \quad (A4)$$

It is valid to assume that $f^0 = f_M$ from (A3). Then,

$$f^1_{BGK} = -\frac{\lambda_e}{Z} \left(\frac{\partial f_M}{\partial z} + \frac{q_e E_z}{m_e v} \frac{\partial f_M}{\partial v} \right). \quad (A5)$$

The *quasi-neutrality* constraint, corresponding to a zero current imposed by the electric field reads

$$\boldsymbol{j} \equiv q_e \int \boldsymbol{v} \tilde{f} \, d\boldsymbol{v} = \boldsymbol{0}. \quad (A6)$$

In the case of the BGK EDF, in particular its anisotropic part (A5), the zero current condition takes the form

$$2\pi \int_{-1}^{1} \int_v v \mu^2 f^1_{BGK} \, dv d\mu = 0,$$

which leads to the electric field (same as the classical Lorentz electric field $\boldsymbol{E}_L$ [29])

$$E_z = \frac{m_e v_{th}^2}{q_e} \left(\frac{1}{L_{n_e}} + \frac{5}{2} \frac{1}{L_{T_e}} \right). \quad (A7)$$

It is worth mentioning, that the deviation of f^0 from f_M in (A3) can be written as $\left(\frac{\lambda_e}{L_{n_e}} + \frac{5}{2} \frac{\lambda_e}{L_{T_e}} \right) \frac{v_{th}^2}{v^2} f^1$, where naturally arises the Knudsen number $Kn = \frac{\lambda_e}{L_{n_e}} + \frac{5}{2} \frac{\lambda_e}{L_{T_e}}$ comprising both contributions of electron density and temperature gradients, and that a multiplication of the electron-electron collision contribution can be multiplied by a constant in (A2) without changing the resulting form of the local anisotropic term (A4), and consequently the current and heat flux. This constant will be labeled r as introduced in [50] and the BGK operator (8) can be written as $r\nu_e(\tilde{f} - f_M) + \frac{\nu_{ei} + r\nu_e}{2} \frac{\partial}{\partial \mu} (1 - \mu^2) \frac{\partial \tilde{f}}{\partial \mu}$.

In the case of the AWBS operator (5) used in (7), its action on (6) reads

$$\frac{1}{v} C_{AWBS}(\tilde{f}) = \frac{v\zeta}{\lambda_e} \frac{\partial}{\partial v} \left(\tilde{f} - f_M \right)$$
$$+ \frac{1}{2} \left(\frac{Z}{\lambda_e} + \frac{\zeta}{\lambda_e} \right) \frac{\partial}{\partial \mu} (1 - \mu^2) \frac{\partial \tilde{f}}{\partial \mu}$$
$$= \frac{v\zeta}{\lambda_e} \frac{\partial}{\partial v} \left(f^0 - f_M \right)$$
$$+ \mu \left(\frac{v\zeta}{\lambda_e} \frac{\partial f^1}{\partial v} - \frac{Z + \zeta}{\lambda_e} f^1 \right), \quad (A8)$$

where $\nu_e^* = \zeta \nu_e = \frac{v\zeta}{\lambda_e}$ with ζ being a scaling parameter of the standard e-e collision frequency. Its purpose is to

match AWBS heat flux to results obtained by Spitzer and Harm [5] obtained for any Z. Sec. III C shows that this match can be found with a constant $\zeta = 0.5$.

One finds the following equations if the isotropic and anisotropic parts of (A1) and (A8) are compared

$$\frac{\partial}{\partial v}\left(f^0 - f_M\right) = \frac{\lambda_e q_e E_z}{\zeta m_e v^2}\frac{f^1}{v}, \qquad (A9)$$

$$\frac{v\zeta}{\lambda_e}\frac{\partial f^1}{\partial v} - \frac{Z+\zeta}{\lambda_e}f^1 = \frac{\partial f^0}{\partial z} + \frac{q_e E_z}{m_e v}\frac{\partial f^0}{\partial v}. \qquad (A10)$$

If we assume that $\frac{\partial f^0}{\partial v} = \frac{\partial f_M}{\partial v}$, i.e. $f^0 = f_M$, the anisotropic part of the AWBS operator is governed by the equation

$$\frac{\partial f^1_{AWBS}}{\partial v} - \frac{Z+\zeta}{v\zeta}f^1_{AWBS} = \frac{\lambda_e}{v\zeta}\left(\frac{\partial f_M}{\partial z} + \frac{q_e E_z}{m_e v}\frac{\partial f_M}{\partial v}\right). \qquad (A11)$$

Even though it is not straightforward, the electric field in (A11) (solved numerically) providing a zero current exactly matches (A7). Consequently, the deviation of $\frac{\partial f^0}{\partial v}$ from $\frac{\partial f_M}{\partial v}$ in (A9) can be written as $Kn\frac{v_{th}^2}{\zeta v^2}\frac{f^1}{v}$.

Finally, it should be stressed, that the concept of locality expressed as $Kn \ll 1$ is crucial for our *local diffusive regime* analysis, because it provides sufficient Maxwellization, i.e. (A3) and (A9), and correspondingly, (A5) and (A11) are valid models.

Appendix B: AP1 electric field limit

Interestingly, we have encountered a very specific property of the AP1 model with respect to the electric field magnitude. The easiest way how to demonstrate this is to write the model equations (22) and (23) in 1D (z-axis). Then, due to its linear nature, it is easy to eliminate one of the partial derivatives with respect to v, i.e. $\frac{\partial f_0}{\partial v}$ or $\frac{\partial f_{1z}}{\partial v}$. In the case of elimination of $\frac{\partial f_0}{\partial v}$ one obtains the following equation

$$\left(v\frac{\nu_e}{2} - \frac{2q_e^2 E_z^2}{3m_e^2 v\nu_e}\right)\frac{\partial f_{1_z}}{\partial v} = \frac{2q_e E_z}{3m_e\nu_e}\frac{\partial f_{1_z}}{\partial z} + \frac{4\pi q_e E_z}{3m_e}\frac{\partial f_M}{\partial v}$$
$$+ \frac{v}{3}\frac{\partial f_0}{\partial z} + \left(\frac{4q_e^2 E_z^2}{3m_e^2 v^2\nu_e} + \left(\nu_{ei} + \frac{\nu_e}{2}\right)\right)f_{1_z}. \qquad (B1)$$

It is convenient to write the bracket on the left hand side of (B1) as $\frac{2}{3v\nu_e}\left(\left(\sqrt{3}v\frac{\nu_e}{2}\right)^2 - \frac{q_e^2}{m_e^2}E_z^2\right)$ from where it is clear that the bracket is negative if $\sqrt{3}v\frac{\nu_e}{2} < \frac{q_e}{m_e}|\boldsymbol{E}|$, i.e. there is a velocity limit for a given magnitude $|\boldsymbol{E}|$, when the collisions are no more fully dominant and the electric field introduces a comparable effect to the collision friction in the electron transport.

It can be shown, that the last term on the right hand side of (B1) is dominant and the solution behaves as

$$\Delta\boldsymbol{f_1} \sim \exp\left(\frac{\frac{4q_e^2 E_z^2}{3m_e^2 v^2\nu_e} + \left(\nu_{ei} + \frac{\nu_e}{2}\right)}{v\frac{\nu_e}{2} - \frac{2q_e^2 E_z^2}{3m_e^2 v\nu_e}}\Delta v\right), \qquad (B2)$$

where $\Delta v < 0$ represents a velocity step of the implicit Euler numerical integration of decelerating electrons. However, (B2) exhibits an exponential growth for velocities above the friction limit (bracket on the left hand side of (B1))

$$v_{lim} = \sqrt{\frac{\sqrt{3}\Gamma m_e}{2q_e}\frac{n_e}{|\boldsymbol{E}|}}, \qquad (B3)$$

which makes the problem to be ill-posed.

In order to provide a stable model, we introduce a reduced electric field to be acting as the accelerating force of electrons

$$|\boldsymbol{E}_{red}| = \sqrt{3}v\frac{m_e}{q_e}\frac{\nu_e}{2}, \qquad (B4)$$

ensuring that the bracket on the left hand side of (B1) remains positive. We define a quantity $\eta_{red} = \frac{|\boldsymbol{E}_{red}|}{|\boldsymbol{E}|}$. Then, the AP1 model (22), (23) can be formulated as well posed

$$v\frac{\nu_e}{2}\frac{\partial}{\partial v}\left(f_0 - f_M\right) = \frac{v}{3}\nabla\cdot\boldsymbol{f_1} + \frac{q_e}{m_e}\frac{\boldsymbol{E}}{3}\cdot$$
$$\left(\eta_{red}\frac{\partial\boldsymbol{f_1}}{\partial v} + \frac{2(2-\eta_{red})}{v}\boldsymbol{f_1}\right), \qquad (B5)$$

$$v\frac{\nu_e}{2}\frac{\partial\boldsymbol{f_1}}{\partial v} - \nu_{scat}\boldsymbol{f_1} = v\nabla f_0 + \frac{q_e\eta_{red}}{m_e}\boldsymbol{E}\frac{\partial f_0}{\partial v} + \frac{q_e\boldsymbol{B}}{m_e c}\times\boldsymbol{f_1}, \qquad (B6)$$

while introducing the reduction factor of the accelerating electric field and the compensation of the electric field effect via its angular term.

[1] R. S. Cohen, L. Spitzer, Jr., P. M. Routly, The electrical conductivity of an ionized gas, Phys. Rev. 80 (1950) 230–238.

[2] J. H. Jeans, Astronomy and Cosmogony, Cambridge University Press, London, 1929.

[3] S. Chandrasekhar, Stochastic problems in physics and astronomy, Rev. Mod. Phys. 15 (1943) 1.

[4] M. Planck, Über einen Satz der statistischen Dynamik und seine Erweiterung in der Quantentheorie, Sitzungsber. Preuss. Akad. Wiss. 24 (1917) 324–341.

[5] L. Spitzer, Jr. and R. Härm, Transport phenomena in a completely ionized gas, Phys. Rev. 89 (1953) 977.

[6] J. H. Jeans, The equations of radiative transfer of energy, Month. Not. Royal Astr. Soc. 78 (1917) 28–36.

[7] M. N. Rosenbluth, W. M. MacDonald, D. L. Judd, Fokker-planck equation for an inverse-square force, Phys. Rev. 107 (1957) 1.

[8] A. R. Bell, R. G. Evans, D. J. Nicholas, Phys. Rev. Lett. 46 (1981) 243.

[9] J. P. Matte, J. Virmont, Electron heat transport down steep temperature gradients, Phys. Rev. Lett. 49 (1982) 1936–1939.

[10] S. I. Braginskii, Transport processes in a plasma, Reviews of Plasma Physics 1 (1965) 205.

[11] J. Hawreliak, D. M. Chambers, S. H. Glenzer, A. Gouveia, R. J. Kingham, R. S. Marjoribanks, P. A. Pinto, O. Renner, P. Soundhauss, S. Topping, E. Wolfrum, P. E. Young, J. S. Wark, Thomson scattering measurements of heat flow in a laser-produced plasma, Journal of Physics B: Atomic, Molecular and Optical Physics 37 (7) (2004) 1541.

[12] C. P. Ridgers, R. J. Kingham, A. G. R. Thomas, Magnetic cavitation and the reemergence of nonlocal transport in laser plasmas, Phys. Rev. Lett. 100 (2008) 075003.

[13] L. Willingale, A. G. R. Thomas, P. M. Nilson, M. C. Kaluza, S. Bandyopadhyay, A. E. Dangor, R. G. Evans, P. Fernandes, M. G. Haines, C. Kamperidis, R. J. Kingham, S. Minardi, M. Notley, C. P. Ridgers, W. Rozmus, M. Sherlock, M. Tatarakis, M. S. Wei, Z. Najmudin, K. Krushelnick, Fast advection of magnetic fields by hot electrons, Phys. Rev. Lett. 105 (2010) 095001.

[14] J. J. Bissell, C. P. Ridgers, R. J. Kingham, Field compressing magnetothermal instability in laser plasmas, Phys. Rev. Lett. 105 (2010) 175001.

[15] A. S. Joglekar, A. G. R. Thomas, W. Fox, A. Bhattacharjee, Magnetic reconnection in plasma under inertial confinement fusion conditions driven by heat flux effects in ohm's law, Phys. Rev. Lett. 112 (2014) 105004.

[16] A. S. Joglekar, C. P. Ridgers, R. J. Kingham, A. G. R. Thomas, Kinetic modeling of nernst effect in magnetized hohlraums, Phys. Rev. E 93 (2016) 043206.

[17] R. J. Henchen, M. Sherlock, W. Rozmus, J. Katz, D. Cao, J. P. Palastro, D. H. Froula, Observation of nonlocal heat flux using thomson scattering, Phys. Rev. Lett. 121 (2018) 125001. doi:10.1103/PhysRevLett.121.125001. URL https://link.aps.org/doi/10.1103/PhysRevLett.121.125001

[18] A. Thomas, M. Tzoufras, A. Robinson, R. Kingham, C. Ridgers, M. Sherlock, A. Bell, A review of vlasov-fokkerplanck numerical modeling of inertial confinement fusion plasma, Journal of Computational Physics 231 (3) (2012) 1051 – 1079.

[19] J. R. Albritton, E. A. Williams, I. B. Bernstein, K. P. Swartz, Nonlocal electron heat transport by not quite maxwell-boltzmann distributions, Phys. Rev. Lett. 57 (1986) 1887–1890.

[20] R. J. Kingham, A. R. Bell, An implicit Vlasov-Fokker-Planck code to model non-local electron transport in 2-D with magnetic fields, J. Comput. Phys. 194 (194) (2004) 1–34.

[21] F. Perez, L. Gremillet, A. Decoster, M. Drouin, E. Lefebvre, Improved modeling of relativistic collisions and collisional ionization in particle-in-cell codes, Phys. Plasmas 19 (2012) 083104.

[22] L. Landau, Kinetic equation for the coulomb effect, Phys. Z. Sowjetunion 10 (1936) 154.

[23] N. J. Fisch, Theory of current drive in plasmas, Rev. Mod. Phys. 59 (1987) 175.

[24] D. D. Sorbo, J.-L. Feugeas, P. Nicolai, M. Olazabal-Loume, B. Dubroca, S. Guisset, M. Touati, V. Tikhonchuk, Reduced entropic model for studies of multidimensional nonlocal transport in high-energy-density plasmas, Phys. Plasmas 22 (2015) 082706.

[25] D. D. Sorbo, J.-L. Feugeas, P. Nicolai, M. Olazabal-Loume, B. Dubroca, V. Tikhonchuk, Extension of a reduced entropic model of electron transport to magnetized nonlocal regimes of high-energy-density plasmas, Laser Part. Beams 34 (2016) 412–425.

[26] J. F. Luciani, P. Mora, J. Virmont, Nonlocal heat transport due to steep temeperature gradients, Phys. Rev. Lett. 51 (1983) 1664–1667.

[27] P. Bhatnagar, E. Gross, M. Krook, A Model for Collision Processes in Gases. I. Small Amplitude Processes in Charged and Neutral One-Component Systems, Phys. Rev. 94 (1954) 511–525.

[28] I. P. Shkarofsky, T. W. Johnston, M. P. Bachynskii, The particle Kinetics of Plasmas, Addison-Wesley, Reading, 1966.

[29] H. A. Lorentz, The motion of electrons in metallic bodies, in: Proceedings of the Royal Netherlands Academy of Arts and Sciences, Amsterdam, Vol. 7, 1905, pp. 438–453.

[30] E. M. Epperlein, R. W. Short, A practical nonlocal model for electron heat transport in laser plasmas, Phys. Fluids B 3 (1991) 3092–3098.

[31] I. P. Shkarofsky, Heat conduction and magnetic field induction in the presence of cold-and hot-electron maxwellian distributions, Phys. Rev. Lett. 42 (1979) 1342.

[32] J. F. Luciani, P. Mora, A. Bendib, Magnetic field and nonlocal transport in laser-created plasmas, Phys. Rev. Lett. 55 (1985) 2421–2424.

[33] J. P. Brodrick, M. Sherlock, W. A. Farmer, A. S. Joglekar, R. Barrois, J. Wengraf, J. J. Bissell, R. J. Kingham, D. D. Sorbo, M. P. Read, C. P. Ridgers, Incorporating kinetic effects on nernst advection in inertial fusion simulations, Plasma Physics and Controlled Fusion 60 (8) (2018) 084009.

[34] R. J. Kingham, A. R. Bell, Nonlocal magnetic-field generation in plasmas without density gradients, Phys. Rev. Lett. 88 (2002) 045004. doi:10.1103/PhysRevLett.88.045004. URL https://link.aps.org/doi/10.1103/PhysRevLett.88.045004

[35] M. Holec, J. Limpouch, R. Liska, S. Weber, High-order discontinuous Galerkin nonlocal transport and energy equations scheme for radiation hydrodynamics, Int. J. Numer. Meth. Fl. 83 (2017) 779.

[36] M. Holec, J. Nikl, S. Weber, Nonlocal transport hydrodynamic model for laser heated plasmas, Phys. Plasmas 25 (2018) 032704.

[37] A. B. Langdon, Nonlinear inverse bremsstrahlung and heated-electron distributions, Phys. Rev. Lett. 44 (1980) 575–579.

[38] C. P. Ridgers, A. G. R. Thomas, R. J. Kingham, A. P. L. Robinson, Transport in the presence of inverse bremsstrahlung heating and magnetic fields, Physics of Plasmas 15 (9) (2008) 092311.

[39] T. Group, SESAME report on the Los Alamos equation-of-state library, Tech. Rep. Tech. Rep. LALP-83-4, Los Alamos National Laboratory, Los Alamos (1983).

[40] S. P. Lyon, J. D. Johnson, SESAME: The Los Alamos na-

tional laboratory equation of state database, Tech. Rep. LA-UR-92-3407, Los Alamos National Laboratory, Los Alamos (1992).

[41] V. Dobrev, T. Kolev, R. Rieben, High-order curvilinear finite element methods for Lagrangian hydrodynamics, SIAM J. Sci. Comput. 34 (2012) B606–B641.

[42] MFEM: Modular finite element methods, `mfem.org`.

[43] M. Touati, J.-L. Feugeas, P. Nicolai, J. Santos, L. Gremillet, V. Tikhonchuk, A reduced model for relativistic electron beam transport in solids and dense plasmas, New J. Phys. 16 (2014) 073014.

[44] R. C. Malone, R. L. McCroy, R. L. Morse, Phys. Rev. Lett. 34 (1975) 721.

[45] D. G. Colombant, W. M. Manheimer, M. Busquet, Test of models for electron transport in laser produced plasmas, Phys. Plasmas 12 (2005) 072702.

[46] A. V. Brantov, V. Y. Bychenkov, V. T. Tikhonchuk, Nonlocal electron transport in laser heated plasmas, Phys. Plasmas 5 (1998) 2742–2753.

[47] G. Schurtz, P. Nicolai, M. Busquet, A nonlocal electron conduction model for multidimensional radiation hydrodynamics codes, Phys. Plasmas 4238 (2000) 7.

[48] A. Marocchino and M. Tzoufras and S. Atzeni and A. Schiavi and Ph. Nicolai and J. Mallet and V. Tikhonchuk and J.-L. Feugeas, Comparison for non-local hydrodynamic thermal conduction models, Phys. Plasmas 20 (2013) 022702.

[49] M. Sherlock, J. P. Brodrick, C. P. Ridgers, A comparison of non-local electron transport models for laser-plasmas relevant to inertial confienement fusion, Phys. Plasmas 24 (2017) 082706.

[50] J. P. Brodrick, R. J. Kingham, M. M. Marinak, M. V. Patel, A. V. Chankin, J. T. Omotani, M. V. Umansky, D. D. Sorbo, B. Dudson, J. T. Parker, G. D. Kerbel, M. Sherlock, C. P. Ridgers, Testing nonlocal models of electron thermal conduction for magnetic and inertial confinement fusion applications, Phys. Plasmas 24 (2017) 092309.

[51] G. Schurtz, P. Nicolai, M. Busquet, A nonlocal electron conduction model for multidimensional radiation hydrodynamics codes, Phys. Plasmas 7 (2000) 4238–4249.

[52] S. T. Beliaev, G. I. Budker, The Relativistic Kinetic Equation, Soviet Physics Doklady 1 (1956) 218.

[53] E. Lefebvre, et al, Nucl. Fusion 43 (2003) 629.

[54] T. W. Johnston, Cartesian tensor scalar product and spherical harmonic expansions in boltzmann's equation, Phys. Rev. 120 (1960) 1103–1111.